Sudden emergence of a shallow aragonite saturation horizon in the Southern Ocean

Gabriela Negrete-García[1*], Nicole S. Lovenduski[1], Claudine Hauri[2], Kristen M. Krumhardt[1] & Siv K. Lauvset[3,4]

[1]*Department of Atmospheric and Oceanic Sciences and Institute of Arctic and Alpine Research, University of Colorado Boulder, Boulder, Colorado, USA.*

[2]*International Arctic Research Center, University of Alaska Fairbanks, Fairbanks, AK, USA.*

[3]*NORCE Norwegian Research Centre, Bjerknes Centre for Climate Research, Bergen, Norway*

[4]*Geophysical Institute, University of Bergen and Bjerknes Centre for Climate Research, Bergen, Norway.*

* *now at Scripps Institution of Oceanography, La Jolla, California, USA*

Models project that with current CO_2 emission rates, the Southern Ocean surface will be undersaturated with respect to aragonite by the end of the 21^{st} century[1–4], resulting in widespread impacts on biogeochemistry and ocean ecosystems[5–7]. Particularly concerning is the health of aragonitic organisms, such as pteropods[7], which can dominate surface water communities in polar regions[6]. Here, we quantify the depth of the present-day Southern Ocean aragonite saturation horizon using hydrographic and ocean carbon chemistry observations, and track its evolution over the next century using output from a large ensemble of simulations with a single Earth System Model[8,9]. A new, shallow aragonite saturation horizon emerges in many locations in the Southern Ocean between now and the end of the century. While the emergence of this new horizon is captured by all ensemble members, internal climate variability may affect the year of emergence; thus, its detection may have been overlooked by ensemble average analysis in the past. The emergence of the new horizon is driven by the slow accumulation of anthropogenic CO_2 in the thermocline of the Southern Ocean, where the carbonate ion concentration exhibits a local minimum and approaches undersaturation. The new horizon is apparent under the RCP4.5 emission-stabilizing scenario, as well, indicating an inevitable change. Our results suggest that there will be a sudden decrease in the volume of suitable habitat for aragonitic organisms.

Rising atmospheric carbon dioxide (CO_2) levels resulting from the burning of fossil fuel and industrial and agricultural activities have been abated by CO_2 uptake by the ocean, which has absorbed nearly a third of the total anthropogenic carbon added to the atmosphere[10–12]. As the ocean absorbs atmospheric CO_2, its pH and carbonate ion concentration ($[CO_3^{2-}]$) decrease, thereby decreasing the saturation state ($\Omega = [Ca^{+}][CO_3^{2-}]/K_{sp}$) of calcium carbonate ($CaCO_3$)

minerals aragonite (Ar) and calcite (Ca). Ω_{Ar} and Ω_{Ca} are defined as the ratio of the concentration of dissolved carbonate ions in a given solution to the concentration of dissolved ions in a saturated solution of aragonite and calcite, respectively. Aragonite and calcite are thermodynamically favored to dissolve once Ω falls below the thermodynamic threshold $\Omega = 1$ and the depth at which this happens within the water column is referred to as the saturation horizon. Ocean acidification makes it harder for marine calcifying organisms (e.g. pteropods, corals, coccolithophores, or foraminifera) to form and maintain their shells[1,7,13]. While pteropods exhibit a physiological negative response between $\Omega_{Ar} = 0.94$ and $\Omega_{Ar} = 1.12$[7], soft clams, for example, are sensitive to a decrease in Ω_{Ar} (Figure S5) well above this thermodynamic threshold[14].

The Southern Ocean, defined as the region stretching from the Antarctic coastline to 40°S, is especially vulnerable to the effects of acidification relative to lower latitudes. Here, colder temperatures enhance the solubility of CO_2 and persistent upwelling brings carbon-rich water to the surface ocean[1,3,15]. With current CO_2 emission rates, models project that the Southern Ocean's surface will be undersaturated with respect to aragonite by the end of the 21^{st} century[1,2,10]. This suggests that key marine calcifying organisms, such as those listed above, may not be able to cope well with future environmental conditions, which could change food web dynamics and have cascading effects on global ocean ecosystems[3,13,15]. Ecosystem impacts in the Southern Ocean will serve as a bellwether for prospective impacts at mid and low latitudes where ocean acidification is projected to occur more slowly[3].

Here, we use annual output from the Community Earth System Model Large Ensemble (CESM-LE)[8,9] to study the evolution of the aragonite saturation state under the high-emission Representative Concentration Pathway 8.5 (RCP8.5)[16] scenario (see methods). The CESM is a state-of-the-art coupled climate model that simulates a unique climate trajectory in each ensemble member[8]. The large ensemble enables a robust estimate of the model's forced response to a given emission scenario and an evaluation of the spread in the response due to internal variability. We focus on the change in the saturation state of the $CaCO_3$ mineral aragonite, since it is more soluble than calcite at all temperatures and pressures in the ocean and will reach undersaturation earlier.

The depth of the present day (defined throughout this work as year 2002) observed Southern Ocean aragonite saturation horizon exceeds 1000 m across most of the basin. Within the core of the Antarctic Circumpolar Current (ACC), we find shallower saturation horizons($\sim$400 m; Figure 1a). The upwelling of deep water, which contains high CO_2 concentrations from remineralized organic matter, leads to elevated concentrations of dissolved inorganic carbon (DIC) and establishes a naturally shallow saturation horizon in the core of the ACC[17,18]. The deepest aragonite saturation horizon depths ($\sim$1400 m) occur in the southwestern Indian Ocean, northeast of coastal Argentina, and east of New Zealand.

CESM-LE exhibits a deeper present-day aragonite saturation horizon than that identified by the hydrographic and ocean carbon chemistry observations[19,20] (average bias 522 m; Figure S1). To correct for this bias, we employ a procedure that pins the model projections to present-day observed distributions of carbonate chemistry, nutrients, temperature and salinity (see methods). Hereafter, we refer to the bias-corrected model output. This bias correction procedure has been employed in the past with much success[1,11]. Moreover, it allows us to cleanly describe changes in the saturation horizon due to changes in DIC alone.

The CESM-LE ensemble-mean depth of the aragonite saturation horizon, in the locations of the Southern Ocean (south 40°S) where present-day hydrographic data are available, is 83 m in 2100 (Figure 1c), conforming to results of other recent studies[1,2,10]. Annual average surface ocean aragonite undersaturation begins as early as 2006 in a few discrete locations. Aragonite undersaturation is projected across $\sim$20% of the Southern Ocean surface by 2060, across $\sim$60% of the surface by 2080 and $>$80% of the surface by 2100.

The CESM-LE ensemble projects the emergence of a new shallow saturation horizon across many locations in the Southern Ocean. This emergence is indicated by a step-change in saturation horizon depth of 400 m yr^{-1} or greater. In some locations, a step-change of as much as 1000 m in a single year (Figure 2) is projected. The depth and year of emergence varies spatially, reflecting both natural variation in the present-day saturation horizon depth and spatial variability in the physical circulation of the Southern Ocean. In the core of the ACC in the South Atlantic, we observe the largest step-changes in saturation horizon, ranging from 400 to 1000 m yr^{-1} (Figure S2). The step-change is more moderate in the Indian sector, with the exception of a few points near the sea ice edge at 82.5°E. Step-changes of 500 m yr^{-1} or more are found throughout the Pacific Sector, extending into the subtropical latitudes.

The year of emergence of a shallow aragonite saturation horizon can vary across ensemble members, owing to their different representations of internal variability (Figure 2, Figure S2), such as ENSO and the Southern Annular Mode which can affect surface $[CO_3^{2-}]$[21,22]. For example, Figure 2a illustrates that while all ensemble members project the emergence of a shallow saturation horizon at 0.5°E and 52.5°S, the year of emergence occurs as early as 2006 in one ensemble member and as late as 2038 in another. This internally-driven spread in the year of emergence means that the average change in the saturation horizon (the mean across all ensemble members) is more moderate at this location. Similar conclusions can be drawn at other locations (Figures 2b-e), suggesting that using the ensemble mean of several projections from one or more models (as is common practice in the Intergovernmental Panel on Climate Change reports and related publications) may mis-represent the emergence of a shallow horizon and the critical depth where this occurs.

The emergence of a shallow aragonite saturation horizon can be explained by the slow accumulation of anthropogenic carbon in the Southern Ocean thermocline that drives a local reduction of $[CO_3^{2-}]$ at the $[CO_3^{2-}]$ minimum (Figure 3). The highest concentrations of $[CO_3^{2-}]$ are naturally found in the surface ocean and the lowest concentrations in the bottom of the water column, with a local minimum in the thermocline (Figure 3c). This $[CO_3^{2-}]$ distribution reflects the imprint of surface photosynthesis and thermocline remineralization on the DIC concentration; photosynthesis draws down DIC and increases $[CO_3^{2-}]$, while remineralization produces DIC and decreases $[CO_3^{2-}]$[23]. In the Southern Ocean, the thermocline minimum in $[CO_3^{2-}]$ approaches the saturation concentration for mineral aragonite ($[CO_3^{2-}]_{sat(arag)}$); which is primarily a function of pressure and increases with depth in the ocean[23] (Figure 3c). Thus, an incremental addition of anthropogenic DIC to the thermocline has the potential to lower the $[CO_3^{2-}]$ below the critical $[CO_3^{2-}]_{sat(arag)}$ threshold, creating a sudden $\Omega = 1$ horizon in the thermocline. This is illustrated at 0.5°E and 52.5°S, where a small increase in thermocline DIC from 2041 to 2042 causes a new saturation horizon to appear at a depth at 200 m (Figure 3). Locations that fall within the region impacted by projected sea ice melt (e.g., 32.5°E and -65.5°S, Figure 2d), lack the carbonate ion minimum in the thermocline. Rapid undersaturation of surface waters here is driven by the invasion of anthropogenic DIC and/or by changes in the distribution of natural DIC as rapid ocean warming and freshening affects stratification and ventilation. Because of the technique we used to propagate the bias correction (see methods), internal variability and externally-forced changes in temperature, salinity, alkalinity, and nutrients have no direct consequences on the depth of the horizon. However, internally- and externally-driven changes in ocean circulation can affect the interior ocean distribution of DIC and thus indirectly impact the depth of the aragonite saturation horizon.

An ensemble of CESM simulations run under the stabilizing-emission scenario RCP4.5 suggests that the emergence of a shallow saturation horizon is unavoidable across a large swath of the Southern Ocean, although the year of emergence can be delayed substantially (Figure 4). This medium ensemble (CESM-ME, so-called because it has 9 ensemble members, see methods) simulates a similar range of internal variability in the depth of the saturation horizon, but with a slower increase in anthropogenic DIC in the Southern Ocean thermocline than that of CESM-LE (RCP8.5). The emergence of a shallow aragonite saturation horizon (defined as the first year where a step-change of saturation horizon is greater than 500 m yr^{-1}) occurs approximately 20 years later in CESM-ME (RCP4.5) compared to CESM-LE (RCP8.5). Nevertheless, increases in thermocline DIC occur throughout the southern-most South Atlantic and Indian basins, causing the emergence of a shallow horizon in all CESM-ME (RCP4.5) ensemble members (Figure S3). Across the Subtropical South Pacific, where the emergence of shallow saturation horizons were projected in all of the CESM-LE (RCP8.5) ensemble members by 2080 (Figure S2), the CESM-ME (RCP4.5) shows no emergence of a shallow horizon (Figure S3), likely because it occurs later than 2080 (which is the end date for CESM-ME simulations).

Our analysis implies that Southern Ocean acidification-sensitive organisms will experience a sudden decrease in the volume of their suitable habitat, including shelled pteropods[1,5–7], foraminifers, cold-water corals[3,24], sea urchins, molluscs[3], and coralline algae[1,3,24]. Shelled pteropods, the major planktonic producers of aragonite, might be especially vulnerable to these changing conditions since they typically live in the upper 300 m and form an integral component of polar and subpolar food webs[5–7]. Pteropods account for a large portion of the flux of calcium carbonate to the deep ocean in the Southern Ocean[25,26], and therefore a decrease in pteropod populations would decrease the amount of calcium carbonate (and, thus, alkalinity) exported to depth. Increased alkalinity remaining in the upper ocean could allow increased oceanic absorption of atmospheric CO_2, an important negative feedback on climate change. Due to the rapid progression of ocean acidification, pteropods may have a limited time to adapt to a corrosive environment since they produce only two generations per year[27]. While the emergence of a shallow saturation horizon has been projected in coastal upwelling systems[28], the Southern Ocean is characterized by much lower natural variability in surface ocean [CO_3^{2-}][21,29]. Given this low background variability, organisms in the Southern Ocean may not be able to contend with sudden changes in the volume of their habitat, with far-reaching consequences for fisheries, economies, and livelihoods.

Due to the lack of ship-board wintertime observations, the CESM aragonite saturation horizon is unable to be verified during winter months. Therefore, this analysis focuses only on the annual mean values of aragonite saturation state in the Southern Ocean. Other studies[4,30], however, show an intense surface wintertime minimum in CO_3^{2-} south of the Antarctic Polar Front, which, combined with increasing amounts of anthropogenic CO_2, will likely lead to earlier undersaturation events during winter. Finally, we note that while CESM-LE and -ME do not represent the potential physiological responses of organisms to ocean acidification, such as altered calcification rates, N_2 fixation, and net primary production, these may also cause future changes in local carbonate chemistry with potentially important climate-carbon feedbacks[15].

Methods

Hydrographic and carbon chemistry observations

We use global mapped climatologies of ocean biogeochemical and physical variables collected via hydrographic cruises to identify the present-day Southern Ocean aragonite saturation horizon. DIC and alkalinity are taken from an adaptation of the Global Ocean Data Analysis Product for Carbon, version 2 (GLODAPv2) mapped product[20] that excludes artificial data along the GLODAPv2 mapping boundary at 20°E and includes only data that were quality-controlled (i.e., no profiles with a maximum sampling depth shallower than 1500 m and no profiles without crossovers)[19]. DIC observations were normalized to the year 2002 before mapping, by removing the temporal trends in DIC and pH due to anthropogenic influence[19,20]. We used mapped climatologies of temperature, salinity, silicate, and phosphate from the World Ocean Atlas (WOA) 2009[31–33]. GLODAP and WOA mapped products are on 1° x 1° grids with 33 standard depth surfaces, but here we only used the values in locations where there are observations. We used

Mocsy 1.0[34], a Fortran 90 package that determines the ocean carbonate system, to compute the annual-mean saturation state of aragonite at every location and depth in the Southern Ocean. Mocsy uses DIC, salinity, temperature, alkalinity, phosphate, and silicate in combination with the Lee et al. (2010)[35] formulation for total boron, K_1/K_2 constants from Lueker et al. (2000)[36], and the Dickson and Riley (1979)[37] formulation for K_f to compute carbonate chemistry variables. The saturation horizon was defined at each location as the depth where Ω_{Ar} is nearest 1.

Community Earth System Model ensembles

We project future changes of the aragonite saturation horizon in the Southern Ocean using annual-mean DIC output from the CESM-LE (2006-2100, 32 ensemble members analyzed)[8] and CESM-ME (2006-2080, 9 ensemble members analyzed)[16]. CESM is a state-of-the-art coupled climate model run with atmosphere, ocean (nominal 1^o horizontal resolution and 60 vertical levels), land and sea ice components[38]. All CESM ensemble members are exposed to the same external forcing: historical forcing from 1920 to 2005 and either RCP8.5 (CESM-LE) or RCP4.5 (CESM-ME) from 2006 onward. CESM-LE (RCP8.5) simulations were carried out to 2100, while CESM-ME (RCP4.5) simulations were carried out to 2080. Each ensemble member has a unique climate trajectory because of small round off level differences in their atmospheric initial conditions[8]. All the CESM ensemble members began with an 1850 control simulation with constant pre-industrial forcing. The ocean model physical state was initialized to observations, while the ocean biogeochemical fields were initialized to a state derived from a separate 600-year spin-up. While these spin-ups resulted in a quasi-equilibrium for ocean biogeochemistry, we found significant biases in modeled, present-day Southern Ocean DIC as compared to observations (Figure S1, see also Long et al. (2013)[39]).

We therefore employed the procedure outlined in Orr et al. (2005)[1] and Ciais et al. (2013)[11] to make bias-corrected projections of the Southern Ocean aragonite saturation horizon from the two CESM ensembles. For each ensemble member and each projection year, we interpolated the model output to the GLODAP grid and calculated the annual-mean DIC anomaly relative to the model estimate in 2002. We propagate this bias correction to 2100 in each ensemble member by adding the simulated model perturbations of DIC, relative to 2002, to the GLODAPv2 DIC climatology, while holding alkalinity, nutrients, temperature, and salinity constant. As for the observations (see above), we used Mocsy[34] to calculate the resulting Southern Ocean aragonite saturation state from the bias-corrected DIC model projections. Here too the alkalinity, temperature, salinity, silicate, and phosphate were all held constant at their present-day climatological values.

For a given year and desired depth level, ensemble mean values of the simulated variables were computed by averaging across ensemble members. Areas that on an annual-average are covered in sea ice were omitted from our analysis, due to well known biases in the present-day CESM sea-ice distribution[40]. We define sea ice extent as the northernmost grid point where the simulated sea ice fraction either equals or exceeds 0.2.

Seasonal Bias

Since the Southern Ocean, due to its remoteness and prohibitive wintertime weather, is almost exclusively sampled during austral summer (December - March), the ship-based biogeochemical observations in GLODAPv2 contain a seasonal bias and very few grid points have data from all seasons. Even when data are available from all seasons, they are often collected many years apart, and these inter-annual variations challenge our ability to identify true seasonal variability. Despite studies showing that seasonal variations of temperature, surface mixed layer depth, and spring blooms have a noticeable impact on Ω_{Ar} and Ω_{Ca} in some regions of the global oceans[41], no attempt has been made to correct for this seasonal bias in the GLODAPv2 mapped climatologies. This is due both to limited data coverage, and that such corrections would have to rely on relationships with ancillary variables and different temporal gap-filling methods[20]. The seasonal measurement bias remains one of the largest sources of unquantified uncertainty for the Ω_{Ar} and Ω_{Ca} estimates in the GLODAPv2 mapped climatologies.

References

1. Orr, J. C. *et al.* Anthropogenic ocean acidification over the twenty-first century and its impact on calcifying organisms. *Nature* **437**, 681–686 (2005). URL http://dx.doi.org/10.1038/nature04095.

2. Hauri, C., Friedrich, T. & Timmermann, A. Abrupt onset and prolongation of aragonite undersaturation events in the Southern Ocean. *Nature Climate Change* **6**, 172–176 (2016). URL http://dx.doi.org/10.1038/NCLIMATE2844.

3. Fabry, V. J., McClintock, J. B., Mathis, J. T. & Grebmeier, J. M. Ocean Acidification at High Latitudes: The Bellwether. *Oceanography* **22**, 160–171 (2009). URL `http://dx.doi.org/10.5670/oceanog.2009.105`.

4. McNeil, B. I. & Matear, R. J. Southern Ocean acidification: A tipping point at 450-ppm atmospheric co$_2$. *Proceedings of the National Academy of Sciences* **105**, 18860–18864 (2008). URL `http://dx.doi.org/10.1073/pnas.0806318105`.

5. Moy, A. D., Howard, W. R., Bray, S. G. & Trull, T. W. Reduced calcification in modern Southern Ocean planktonic foraminifera. *Nature Geoscience* **2**, 276–280 (2009). URL `http://dx.doi.org/10.1038/NGEO460`.

6. Hunt, B. *et al.* Pteropods in Southern Ocean ecosystems. *Progress in Oceanography* **78**, 193–221 (2008). URL `http://dx.doi.org/10.1016/j.pocean.2008.06.001`.

7. Bednaršek, N. *et al.* Extensive dissolution of live pteropods in the Southern Ocean. *Nature Geoscience* **5**, 881–885 (2012). URL `http://dx.doi.org/10.1038/NGEO1635`.

8. Kay, J. E. *et al.* The Community Earth System Model (CESM) Large Ensemble Project: A Community Resource for Studying Climate Change in the Presence of Internal Climate Variability. *Bulletin of the American Meteorological Society* **96**, 1333–1349 (2015). URL `https://doi.org/10.1175/BAMS-D-13-00255.1`.

9. Lovenduski, N. S., McKinley, G. A., Fay, A. R., Lindsey, K. & Long, M. C. Partitioning uncertanty in ocean carbon uptake projections: Internal variability, emission scenario, and model structure. *Global Biogeochemical Cycles* **30**, 1276–1287 (2016). URL `https://doi.org/10.1002/2016GB005426`.

10. Feely, R. A. *et al.* Impact of Anthropogenic CO_2 on Impact of Anthopogenic CO_2 on the $CaCO_3$ System in the Oceans. *Science* **305**, 362–366 (2004). URL `http://science.sciencemag.org/content/305/5682/362`.

11. Cais, P. *et al.* Carbon and Other Biogeochemical Cycles supplementary material. in: Climate change 2013: The physical science basis. contribution of working group i to the fifth assessment report of the intergovernmental panel on climate change [stocker, t.f., d. qin, g.-k. plattner, m. tignor, s.k. allen, j. boschung, a. nauels, y. xia, v. bex and p.m. midgley (eds.)]. *Climate Change 2013: The Physical Science Basis.* (2013). URL `www.climatechange2013.org`.

12. Le Quere, C. *et al.* Global Carbon Buget 2017. *Earth System Science Data* **10**, 405–448 (2018). URL `http://doi.org/10.5194/essd-2017-123`.

13. Kroeker, K. J. *et al.* Impacts of ocean acidification on marine organisms: quantifying sensitivities and interaction with warming. *Global Change Biology* **19**, 1884–1896 (2013). URL `http://dx.doi.org/10.1111/gcb.12179`.

14. Ries, J. B., Cohen, A. L. & McCorkle, D. C. Marine calcifiers exhibit mixed responses to co$_2$-induced ocean acidification. *Geology* **37**, 1131–1134 (2009). URL `http://dx.doi.org/10.1130/G30210A.1.` `/gsw/content`$_public/journal/geology/37/12/10.1130_g30210a.1/3/i0091-7613-37-12-1131.pdf$.

15. Doney, S. C., Fabry, V. J., Feely, R. A. & Kleypas, J. A. Ocean Acidification: The Other CO_2 Problem. *Annual Review of Marine Science* **1**, 169–192 (2009). URL http://dx.doi.org/10.1146/annurev.marine.010908.163834.

16. Sanderson, B. M., Oleson, K. W., Strand, W. G., Lehner, F. & O'Neill, B. C. A new ensemble of GCM simulations to assess avoided impacts in a climate mitigation scenario. *Climatic Change* **146**, 303–318 (2015). URL http://dx.doi.org/10.1007/s10584-015-1567-z.

17. Lovenduski, N. S., Gruber, N. & Doney, S. C. Toward a mechanistic understanding of the decadal trends in the Southern Ocean carbon sink. *Global Biogeochemical Cycles* **22** (2008). URL https://agupubs.onlinelibrary.wiley.com/doi/abs/10.1029/2007GB003139.

18. Marshall, J. & Speer, K. Closure of the meridional overturning circulation through Southern Ocean upwelling. *Nature Geoscience* **5**, 171–180 (2012). URL http://dx.doi.org/10.1038/NGEO1391.

19. Olsen, A. *et al.* The Global Ocean Data Analysis Project version 2 (GLODAPv2) – an internally consistent data product for the world ocean. *Earth System Science Data* **8**, 297–323 (2016). URL http://dx.doi.org/10.5194/essd-8-297-2016.

20. Lauvset, S. K. *et al.* A new global interior ocean mapped climatology: the 1^o x 1^o GLODAP version 2. *Earth System Science Data* **8**, 325–340 (2016). URL http://oceanrep.geomar.de/31183/.

21. Conrad, C. J. & Lovenduski, N. S. Climate-Driven Variability in the Southern Ocean Carbonate System. *Journal of Climate* **28**, 5335–5350 (2015). URL http://dx.doi.org/10.1175/JCLI-D-14-00481.1.

22. Xue, L. *et al.* Climatic modulation of surface acidification rates through summertime wind forcing in the southern ocean. *Nature Communications* **9** (2018). URL http://dx.doi.org/10.1038/s41467-018-05443-7.

23. Sarmiento, J. L. & Gruber, N. *Ocean Biogeochemical Dynamics* (Princeton University Press, 41 William Street, Princeton, NJ 08540, 2006).

24. Freiwald, A., Fossa, J. H., Grehan, A., Koslow, T. & Roberts, J. Cold-water Coral Reefs: Out of Sight—No Longer Out of Mind. *Biodiversity Series, UNEP-WCMC, Cambridge, UK* (2004).

25. Honjo, S., Francois, R., Manganini, S. J., Dymond, J. R. & Collier, R. W. Particle flux in the Pacific sector of the Southern Ocean (2000). URL https://doi.org/10.1594/PANGAEA.787552. Supplement to: Honjo, S et al. (2000): Particle fluxes to the interior of the Southern Ocean in the Western Pacific sector along 170°W. Deep Sea Research Part II: Topical Studies in Oceanography, 47(15-16), 3521-3548, https://doi.org/10.1016/S0967-0645(00)00077-1.

26. Honjo, S. Particle export and the biological pump in the Southern Ocean. *Antarctic Science* **16**, 501–516 (2004). URL https://doi.org/10.1017/S0954102004002287.

27. Dadon, J. R. & de Cidre, L. L. The reproductive cycle of the Thecosomatous pteropod Limacina retroversa in the western South Atlantic. *Marine Biology* **114**, 439–442 (1992). URL `https://doi.org/10.1007/BF00350035`.

28. Franco, A. C., Gruber, N., Frölicher, T. L. & Kropuenske Artman, L. Constracting Impact of Future CO_2 Emission Scenatios on the Extent of the $CaCO_3$ Mineral Undersaturation in the Humboldt Current System. *Journal of Geophysical Research: Oceans* **123**, 2018–2036 (2018). URL `https://agupubs.onlinelibrary.wiley.com/doi/abs/10.1002/2018JC013857`.

29. Lovenduski, N. S., Fay, A. R. & McKinley, G. A. Observing multidecadal trends in Southern Ocean co_2 uptake: What can we learn from an ocean model? *Global Biogeochemical Cycles* **29**, 416–426 (2015). URL `https://agupubs.onlinelibrary.wiley.com/doi/abs/10.1002/2014GB004933`.

30. Williams, N. L. *et al.* Assessment of the carbonate chemistry seasonal cycles in the southern ocean from persistent observational platforms. *Journal of Geophysical Research: Oceans* **123**, 4833–4852 (2018). URL `https://agupubs.onlinelibrary.wiley.com/doi/abs/10.1029/2017JC012917`.

31. Locarnini, R. A. *et al.* World Ocean Atlas 2009, Volume 1: Temperature. *S. Levitus, Ed., NOAA Atlas NESDIS 68, U.S. Government Printing Office, Washington, D.C.* 184 (2010).

32. Antonov, J. I. *et al.* World Ocean Atlas 2009, Volume 2: Salinity. *S. Levitus, Ed. NOAA Atlas NESDIS 69, U.S. Government Printing Office, Washington, D.C.* 184 (2010).

33. Garcia, H. E. *et al.* World Ocean Atlas 2009, Volume 4: Nutrients (phosphate, nitrate, and silicate). *S. Levitus, Ed., NOAA Atlas NESDIS 71, U.S. Government Printing Office, Washington, D.C.* 398 (2010).

34. Orr, J. C. & Epitalon, J.-M. Improved routines to model the ocean carbonate system: mocsy 2.0. *Geoscientific Model Development* **8**, 485–499 (2015). URL `http://dx.doi.org/10.5194/gmd-8-485-2015`.

35. Lee, K. *et al.* The universal ratio of boron to chlorinity for the North Pacific and North Atlantic oceans. *Geochimica et Cosmochimica Acta* **74**, 1801 – 1811 (2010). URL `http://www.sciencedirect.com/science/article/pii/S0016703709007789`.

36. Lueker, T. J., Dickson, A. G. & Keeling, C. D. Ocean pco_2 calculated from dissolved inorganic carbon, alkalinity, and equa- tions for k_1 and k_2: validation based on laboratory measurements of co_2 in gas and seawater at equilibrium. *Marine Chemistry* **70**, 105 – 119 (2000). URL `http://www.sciencedirect.com/science/article/pii/S0304420300000220`.

37. Dickson, A. G. & Riley, J. P. The estimation of acid dissociation constants in seawater media from potentiometric titrations with strong base. i. The iconic product of water -k_w. *Marine Chemistry* **7**, 89 – 99 (1979). URL `http://www.sciencedirect.com/science/article/pii/030442037990001X`.

38. Hurrell, J. W. *et al.* The Community Earth System Model: A Framework for Collaborative Research. *Bulletin of the American Meteorological Society* **94**, 1339–1360 (2013). URL `http://dx.doi.org/10.1175/BamS-d-12-00121.1`.

39. Long, M. C., Lindsay, K., Peacock, S., Moore, J. K. & Doney, S. C. Twentieth-Century Oceanic Carbon Uptake and Storage in CESM1(BGC)*. *Journal of Climate* **26**, 6775–6800 (2013). URL `http://dx.doi.org/10.1175/JCLI-D-12-00184.1`.

40. Landrum, L., Holland, M. M., Schneider, D. P. & Hunke, E. Antarctic sea ice climatology, variability, and late twentieth-century change in ccsm4. *Journal of Climate* **25**, 4817–4838 (2012). URL `https://doi.org/10.1175/JCLI-D-11-00289.1`.

41. Jiang, L.-Q. *et al.* Climatological distribution of aragonite saturation state in the global oceans. *Global Biogeochemical Cycles* **29**, 1656–1673 (2015). URL `https://agupubs.onlinelibrary.wiley.com/doi/abs/10.1002/2015GB005198`.

Acknowledgements

We are grateful for support from the National Science Foundation (OCE-1558225, PLR-1543457, OCE -1459834). GNG was supported, in part, by the Significant Opportunities in Atmospheric Research and Science (SOARS) program, NSF grant AGS-1641177. CESM ensemble output is available from the Earth System Grid *(https://www.earthsystemgrid.org/dataset/ucar.cgd.ccsm4.CESM_CAM5.* and *(https://www.earthsystemgrid.org/dataset/ucar.cgd.ccsm4.CESM_CAM5_BGC_ME.html)*. CESM computing resources were provided by CISL at NCAR. We thank B. Medeiros for providing model re-gridding scripts and N. Freeman for helpful comments on an earlier version of the manuscript.

Author contributions statement

N.S.L. and K.M.K. re-gridded the CESM-LE and CESM-ME DIC output to the GLODAP/WOA grid, corrected the model DIC bias, and calculated the aragonite saturation state from the bias-corrected model DIC projections. S.K.L. provided the modified GLODAPv2 mapped climatologies and expertise. G.N.G. analyzed the bias-corrected projections and wrote the manuscript.

All authors were involved in the study design, discussed the results, and helped write the manuscript.

Additional information

Supplementary information is available. Correspondence and requests for materials should be addressed to N.S.L.

Competing financial interests

The authors declare no competing financial interests.

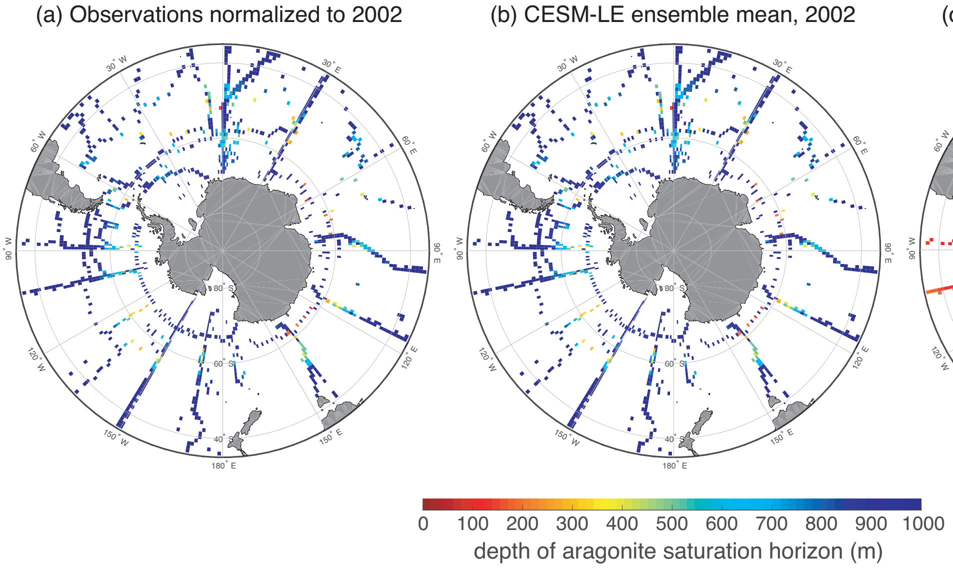

Figure 1: **Depth of Aragonite Saturation Horizon.** Depth of the aragonite saturation horizon from (a) GLODAPv2 bin-averaged DIC (normalized to year 2002) and alkalinity, as well as hydrography data from World Ocean Atlas (WOA2009) sub-sampled at the GLODAPv2 data locations, (b) CESM-LE in 2002, corrected for model bias using hydrographic observations (see methods), and (c) CESM-LE in 2100. Model projections are displayed in 1°x1° grid cells where there are sufficient GLODAPv2 data to identify a present-day saturation horizon.

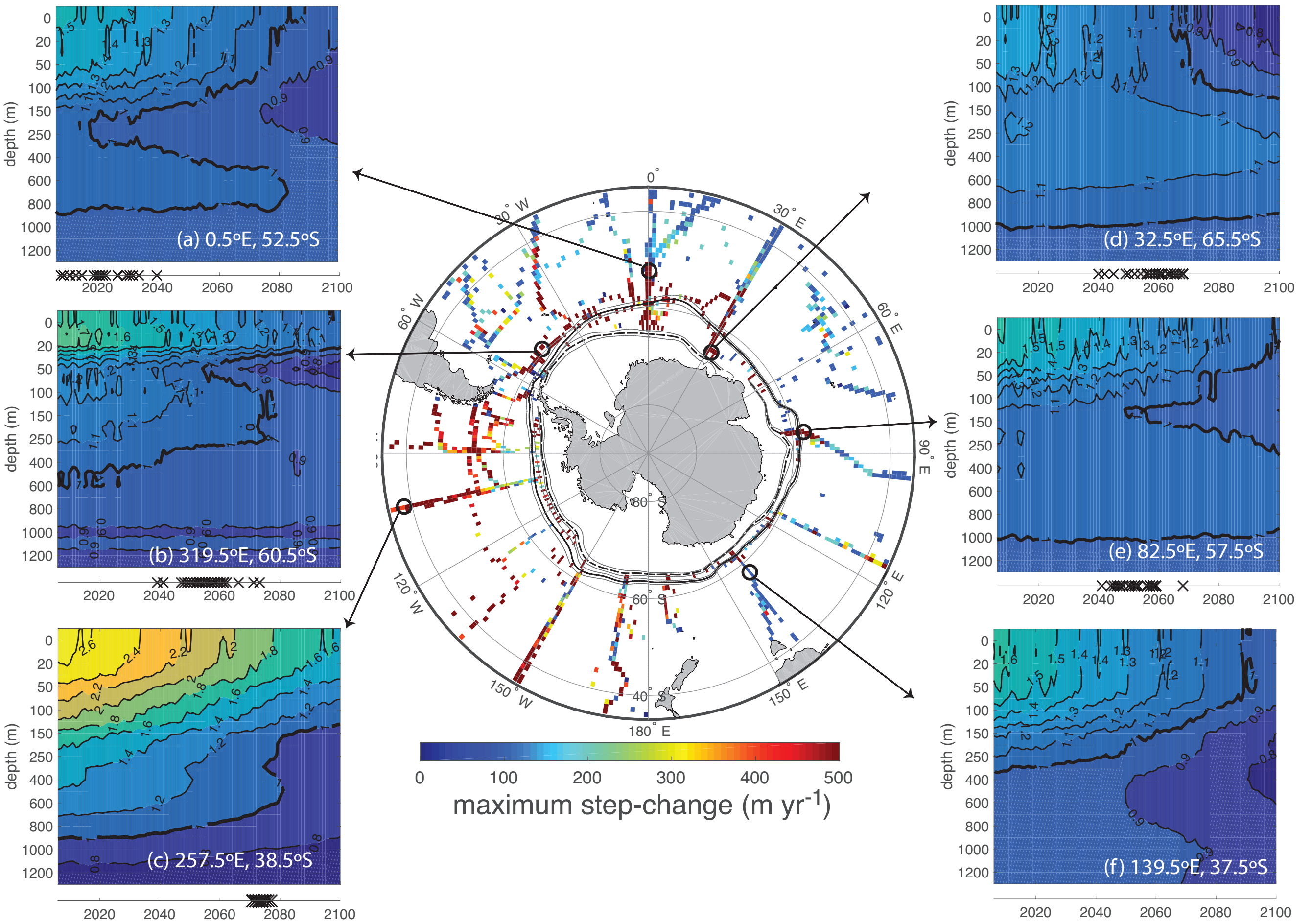

Figure 2: **Emergence of shallow aragonite saturation horizon.** Temporal evolution of upper water column aragonite saturation state in several locations, as projected by a single ensemble member of CESM-LE (RCP8.5): (a) 0.5°E, 52.5°S, (b) 319.5°E, 60.5°S, (c) 257.5°E, 38.5°S, (d) 32.5°E, 65.5°S, (e) 82.5°E, 57.5°S and (f) 139.5°E, 37.5^{o}S. Black X symbols on the time axis correspond to the year in which the new, shallow saturation horizon emerges in individual ensemble members. The center map shows the maximum step-change in aragonite saturation horizon from a single CESM-LE ensemble member over 2006-2100 at each location in the Southern Ocean (m yr^{-1}). Black solid (dashed) line shows the average sea ice extent in 2006 (2100), and thin gray lines show one standard deviation sea ice extent across the CESM-LE ensemble members. Model projections are displayed in 1°x1° grid cells where there are sufficient GLODAPv2 data to identify a present-day saturation horizon.

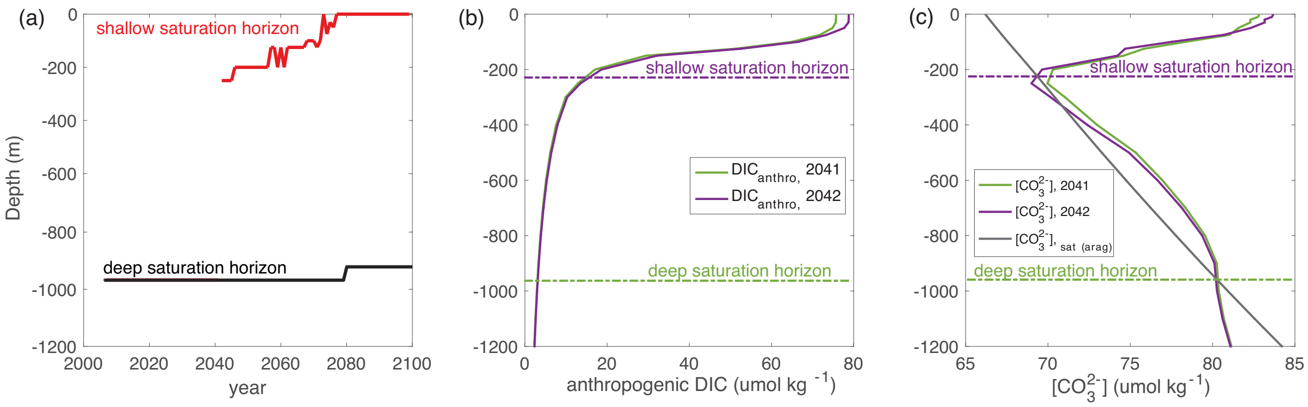

Figure 3: **Why the sudden emergence of shallow horizon?** (a) Temporal evolution of the depth of the aragonite saturation horizon at 0.5°E and 53.5°S from a single CESM-LE ensemble member. Vertical profiles of (b) anthropogenic DIC concentration (μmol kg^{-1}) and the corresponding depth of the aragonite saturation horizon, and (c) carbonate ion concentration (μmol kg^{-1}) from the same location and ensemble member before and after the step-change in aragonite saturation horizon (2041 and 2042, respectively).

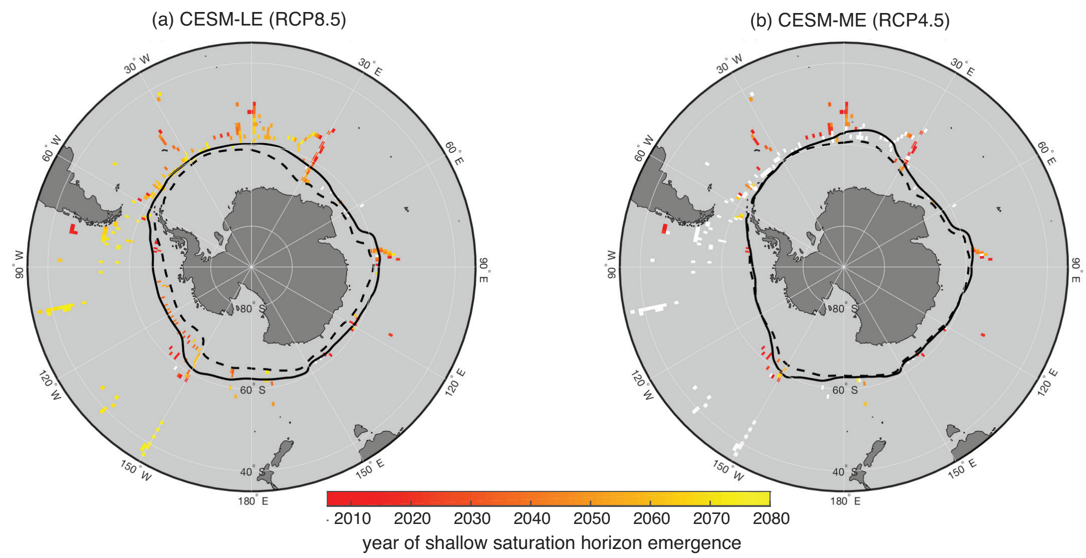

Figure 4: **Year of emergence of shallow saturation horizon.** Projected year of emergence of new, shallow saturation horizons from a single ensemble member under (a) RCP8.5 and (b) RCP4.5 emission scenarios over 2006-2080. The emergence of a shallow saturation horizon is defined as the first year where a step-change in saturation horizon greater than 500 m yr^{-1} occurs. Locations without the emergence of a shallow saturation horizon were omitted. Locations where the emergence of shallow horizons occurs under the high emission scenario, but not the stabilizing emission scenario are shaded white in (b). Black solid (dashed) line shows the average sea ice extent in 2006 (2080). Model projections are displayed in 1°x1° grid cells where there are sufficient GLODAPv2 data to identify a present-day saturation horizon.

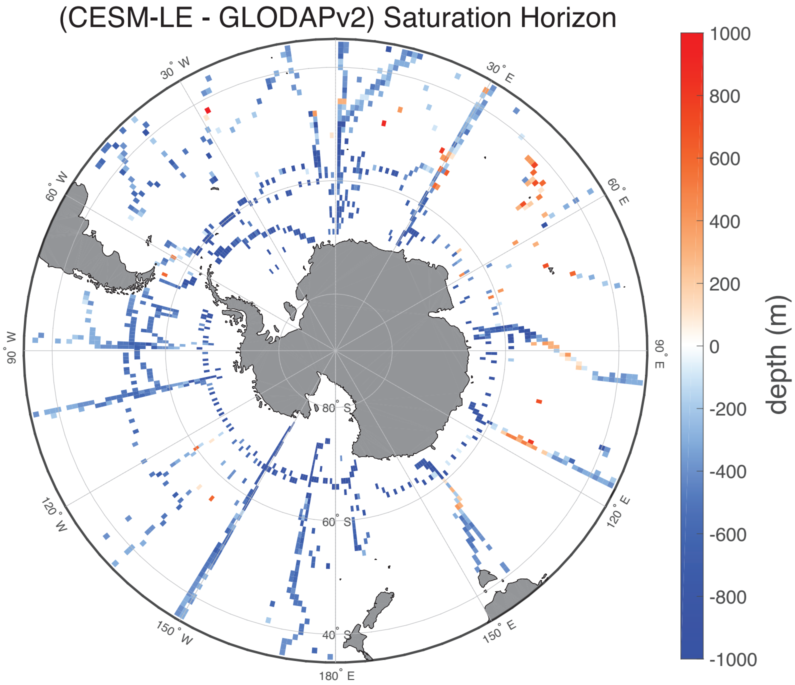

Figure S1: **Model bias.** Ensemble-mean bias in the depth of the present-day aragonite saturation horizon in CESM-LE as compared to GLODAPv2, prior to bias correction.

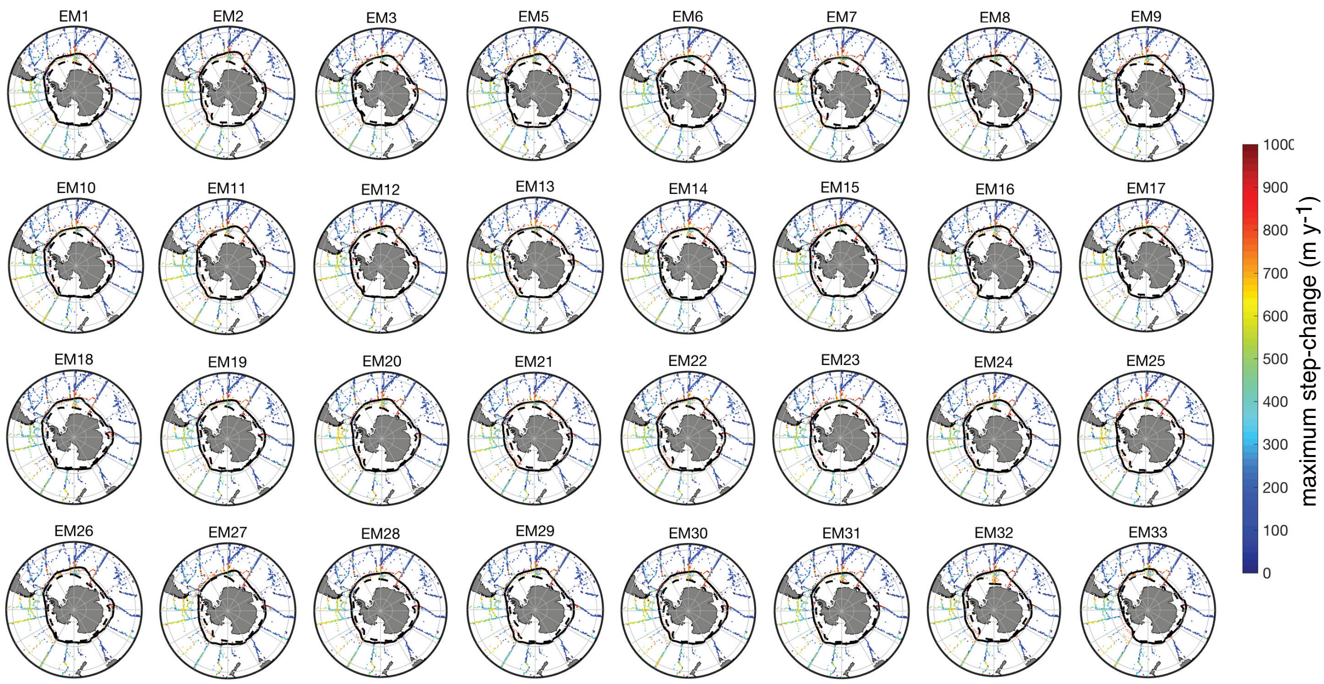

Figure S2: **Ensemble variation in rate of maximum step-change in saturation horizon under RCP8.5.** Maximum step-change of the aragonite saturation horizon for every CESM-LE ensemble member (ensemble member 4 was corrupted) over 2006-2100 (m yr^{-1}). Black solid (dashed) line shows the average sea ice extent in 2006 (2100). Model projections are displayed in 1°x1° grid cells where there are sufficient GLODAPv2 data to identify a present-day saturation horizon. Note different colorbar on Figures 2 and S2.

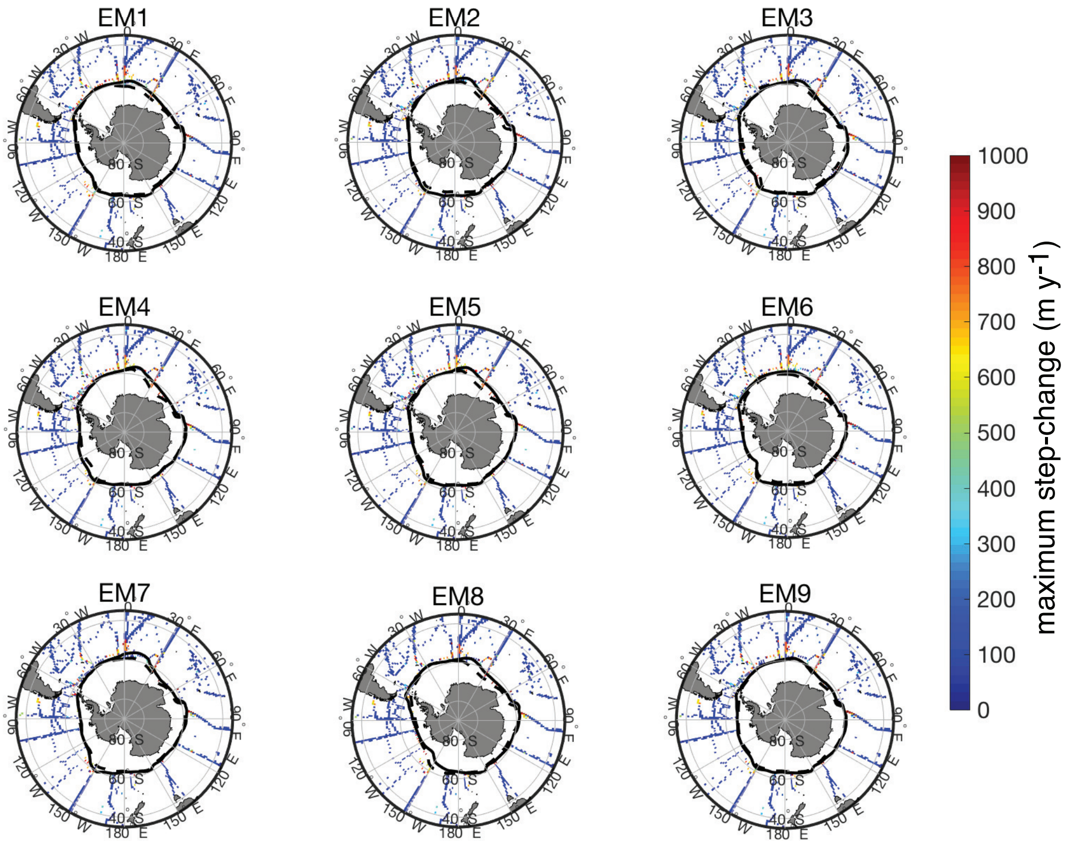

Figure S3: **Ensemble variation in rate of maximum step-change in saturation horizon under RCP4.5.** Maximum step-change of the aragonite saturation horizon for every CESM-ME ensemble member over 2006-2080 (m yr^{-1}). Black solid (dashed) line shows the average sea ice extent in 2006 (2080). Model projections are displayed in 1°x1° grid cells where there are sufficient GLODAPv2 data to identify a present-day saturation horizon.

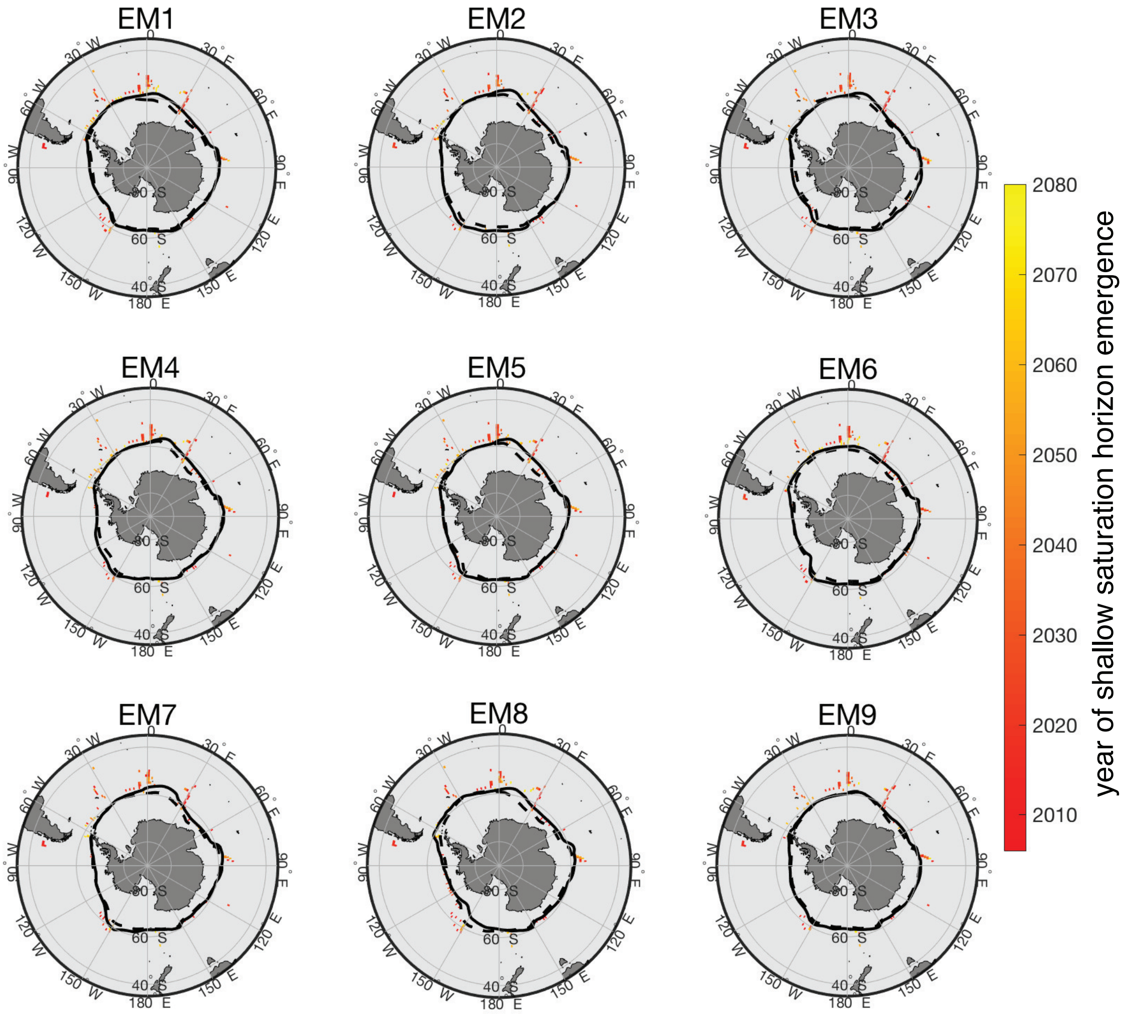

Figure S4: **Ensemble variation in the emergence of shallow horizon under RCP4.5.** Year of emergence of shallow saturation horizon for every CESM-ME ensemble member. The emergence of a shallow saturation horizon is defined as the first year where a step-change in saturation horizon greater than 500 m yr^{-1} occurs. Locations without the emergence of a shallow saturation horizon were omitted. Black solid (dashed) line shows the average sea ice extent in 2006 (2080). Model projections are displayed in 1°x1° grid cells where there are sufficient GLODAPv2 data to identify a present-day saturation horizon.

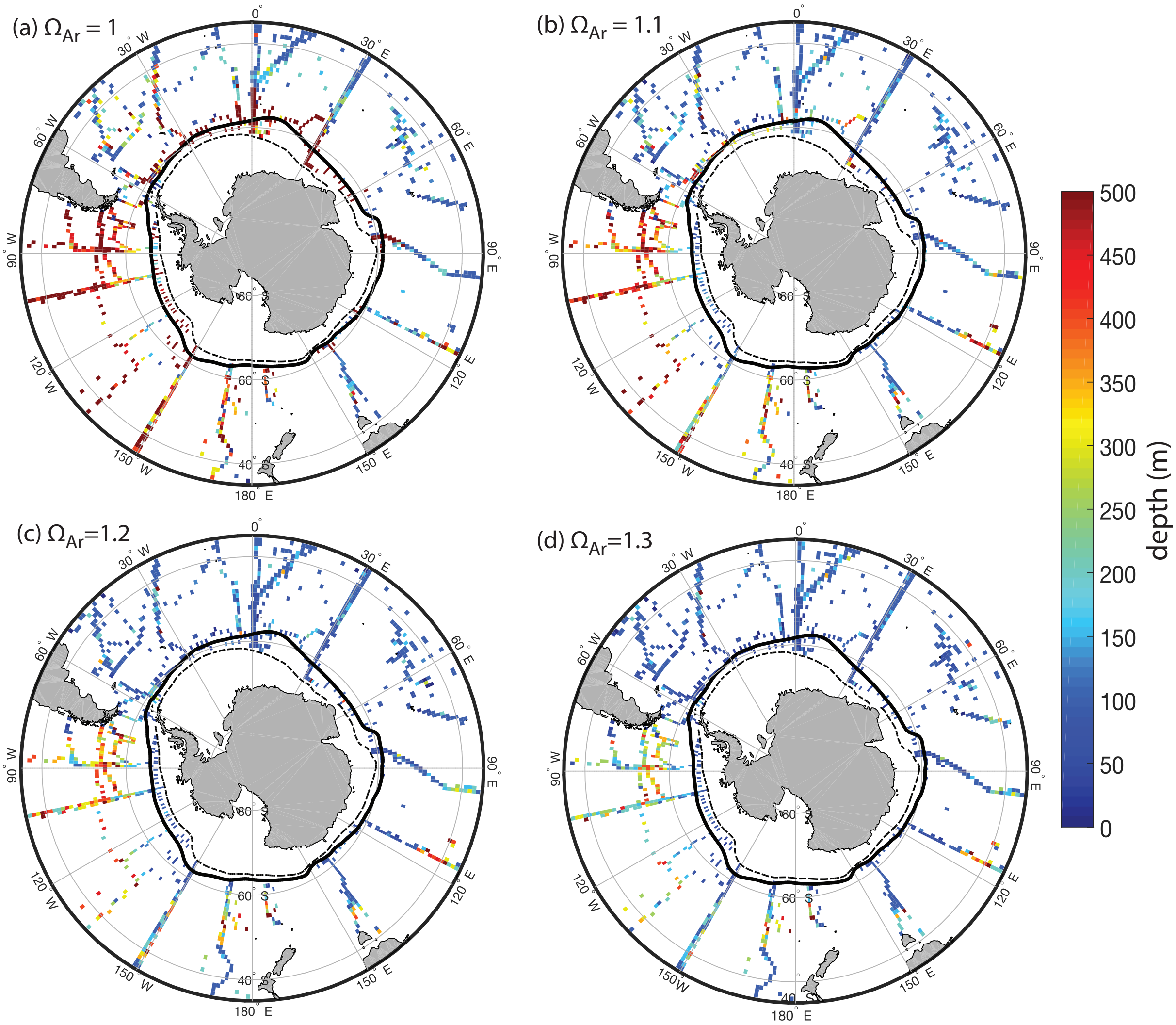

Figure S5: **Rate of maximum step-change in aragonite saturation state.** Rate of maximum step-change for Ω_{Ar} =1,Ω_{Ar} =1.1,Ω_{Ar} =1.2, and Ω_{Ar} =1.3 between two consecutive years. Black solid (dashed) line shows the average sea ice extent in 2006 (2100). Model projections are displayed in 1°x1° grid cells where there are sufficient GLODAPv2 data to identify a present-day saturation horizon.